Supplementary Material for:

On the electrophysiological response of bone cells using a Stokesian fluid stimulus probe for delivery of quantifiable localized picoNewton level forces

Danielle Wu, Peter Ganatos, David C. Spray, & Sheldon Weinbaum

Appendix A – Brief summary of current force probes

A brief summary of the current force probes mentioned in the introduction of the manuscript is given in this appendix. The biomembrane force probe in which a micropipette aspirated red blood cell saturated in streptavidin bonded to a functionalized glass bead decorated to interact with a targeted surface molecule is used in the vertical mode for testing weak bonds under slow loading, and for testing strong bonds under fast loading (Evans and Ritchie, 1997; Evans et al., 2005). To observe biomechanical phenomena at lower forces, optical tweezers are utilized because they are sensitive and accurate at the lower end of the force spectrum from 0-150 pN where a measurable external force is applied to a particle of interest trapped by the laser (Huang et al., 2004; Litvinov et al., 2003). Magnetic pullers and tweezers probes are used to measure local viscoelastic properties of surface adhesion using magnetic bead microrheometry, or magnetic tweezers. These probes generate forces on the order of 4 pN to 10 nN using micron size paramagnetic beads bound to the cell membrane (Bausch et al., 1998; Hu et al., 2004; Hughes et al., 2005). The atomic force microscope (AFM) is a widely used technology for sensitive force measurements to investigate structure of single molecules, surface topography, and mechanical reactions to external forces in the pN range within and between individual biomolecules (Allison et al., 2002; Binnig et al., 1986; Simon and Durrieu, 2006). A horizontal nanomechanical force probe has been developed to combine an AFM cantilever with an optical lever detection module (Ounkomol et al., 2009). This probe measures bond dissociation under tensile forces and serves as a nano- and picoNewton indenter in compression mode with a force resolution of 10-15 pN. A fluid jet from a micropipette was used to estimate the forces required to arrest the migration of a motile cell (Bohnet et al., 2006). However, the fluid jet is turbulent and the forces produced, which are in the nanoNewton range, are difficult to quantify. In the field of calcium imaging, many groups have adopted mechanical indentation with a micropipette as the gold standard for dimpling and poking cells to initiate a release of calcium transients but the forces inducing the response are not readily measured and are believed to be in the nanoNewton range or larger.

Appendix B - Methods Section Extended

Further details and description of select method sections in the main text are provided in this appendix.

2.2.1. Tracer studies

Extracellular solution [mM] - 140 NaCl., 2 CsCl, 2 $CaCl_2$, 1 $MgCl_2$, 5 HEPES, 4 KCL, 5 glucose, 2 Sodium Pyruvate, 1 $BaCl_2$; pH 7.4 using NaOH, filtered using a 0.22 μm pore size bottle top filter (Corning). Lucifer Yellow CH dilithium salt (Sigma-L0259) or Dextran Conjugated Fluorescein (Molecular Probes-D1822) diluted in extracellular solution was used to backfill the micropipette and image the ejected bolus. The bolus is ejected into a glass bottom culture dish (MatTek) by a Picospritzer (Parker) at 20 psi for 100 ms, and analyzed with Metamorph software (Molecular Devices). Positioning of the micropipette was achieved by using the coarse and fine adjustment of a 3-axis hydraulic micromanipulator (SD Instruments).

2.2.3. Laboratory model

A vertically secured 5 mL serological pipette (BD Falcon) was hermetically connected in series to 36 cm of glass tubing, 1.2 m of Teflon FEP tubing (Upchurch Scientific), and the syringe, where the pipette tip was submerged and positioned in the 500 mL reservoir in view of the camera (Sony DSC-W55) to video ejected fluid.

2.3.1. Micropipette setup and placement

Each glass cloverslip with cultured MLO-Y4s was rinsed twice with 1XPBS to rid cells of serum macromolecules before adding extracellular solution for experimentation. The whole-cell voltage-clamp technique is used on each cell prior to SFSP stimulation to record real-time cellular responses. Dendritic MLO-Y4 cells with processes oriented perpendicular to the SFSP micropipette were selected for experiments. See **Figure 2** for force diagram. Micropipette positioning distances were calibrated with the fine adjustment of the 3-axis hydraulic micromanipulator.

2.3.3. Whole-cell voltage-clamp experiments

Patch microelectrodes were pulled as described in Methods Section 2.2.1, but to an initial electrode resistance of 4-5 MΩ, when backfilled with intracellular solution containing [mM] - 130 CsCl, 10 EGTA, 10 HEPES, and 0.5 $CaCl_2$; pH 7.3 with KOH, filtered using a 0.22 μm pore size bottle top filter (Corning). All experiments were performed at room temperature (20-26 °C) using an epi-fluorescent microscope (Nikon), patch clamp amplifier (Axon Instruments), PClamp 8.5 software (Axon Instruments), 3-axis hydraulic micromanipulators (SD Instruments), and a pneumatic vibration isolation table. Recordings from cells with appropriate whole-cell recording seals of high resistance (1-3 GΩ), to eliminate non-specific ionic flux around the microelectrode tip, were extracted from PClamp 8.5 and analyzed in Origin 5.0 (Microcal), ImageJ (NIH), and Prism 5.0 (GraphPad). When more than one cell process response was recorded in a single-cell, the cell process responses were paired with their respective cell body response and analyzed. During an experiment with sequential SFSP loading, the succeeding SFSP pulse is only applied when the membrane potential of the cell has returned to its initial state prior to loading.

Appendix C - Sampson solutions for the velocity and pressure field for the flow through a circular orifice and the growth of its nearly spherical bolus

In this Appendix we provide the solutions for Sampson flow (flow through a circular orifice of radius *c* in a zero thickness plane wall) that have been plotted in **Figure 5b,c,d**. The pressure p_o experienced at the plane of the orifice (micropipette tip) is given by

$$p_0 = p_\infty + \frac{3\mu Q}{2c^3}. \qquad \text{(C1)}$$

Here p_∞ is the fluid pressure far from the tip, μ is the absolute viscosity and *Q* is the volumetric flow rate. The pressure field is given by

$$p = p_0 - (p_0 - p_\infty)\frac{2}{\pi}\left(\frac{\lambda}{\lambda^2+\zeta^2} + \tan^{-1}\lambda\right), \qquad \text{(C2)}$$

where the oblate spheroidal coordinates (λ,ζ) are related to cylindrical coordinates (*r*,*z*) via the relations

$$\lambda^2 = \frac{\beta-\alpha}{2},\ \zeta^2 = \frac{\beta+\alpha}{2},\ \text{where}\ \alpha = 1-\left(\frac{r}{c}\right)^2-\left(\frac{z}{c}\right)^2,\ \beta = \sqrt{\alpha^2+\left(\frac{2z}{c}\right)^2}. \qquad \text{(C3)}$$

Equations (C2) and (C3) provide the isobars shown in **Figure 5d**.

The radial and axial velocity components of the fluid are given by

$$u_r = U_o\frac{\lambda\zeta^2}{\lambda^2+\zeta^2}\sqrt{\frac{1-\zeta^2}{1+\lambda^2}},\quad u_z = U_o\frac{\zeta^2}{\lambda^2+\zeta^2}, \qquad \text{(C4)}$$

where U_o is the centerline velocity in the plane of the orifice given by

$$U_o = \frac{3Q}{2\pi c^2}. \qquad \text{(C5)}$$

The bolus shape at any time t > 0 (**Fig. 5**) is obtained by numerically solving the differential equations for a fluid particle trajectory

$$\frac{dr}{dt} = u_r,\ \frac{dz}{dt} = u_z \qquad \text{(C6)}$$

subject to the initial condition that at t = 0, r = r_0, where $0 \le r_0 \le c$ and $z = 0$. These solutions for bolus growth are shown in the main text for the laboratory scale model where Q = 32.0 mm^3/s (**Fig. 5b**) and for the micropipette ejection where Q = 255 $\mu m^3/ms$ (**Fig. 5c**).

Appendix D – Determination of EI of actin filament bundle and the relationship between the force and the deflection of the cell process

D.1 Determination of the area moment of inertia of the central actin filament bundle

The flexural rigidity *EI* of the central actin filament bundle in the cell process is the product of the Young's modulus *E* of a single actin filament and the area moment of inertia of the actin filament bundle I_b. Calculation of I_b is performed using the parallel axis theorem for multiple bodies where I_a, Equation (D1), is the area moment of inertia for a single actin filament parallel to the line of action through the 5 central actin filaments along the x-axis. The contribution of each actin filament to I_b, Equation (D2), is its area moment of inertia plus the product of the actin's cross sectional area A_a and its squared distance from the line of action. Thus I_b, Equation (D3), is defined as the summation of the contribution of each actin filament in the 19 actin filament hexagonal bundle described in detail in Han et al. (2004) shown in **Figure S1**. In **Figure S1**, r = 2.8 nm and filament spacing a/2 = 12 nm.

Figure S1: Calculation of the area moment of inertia of the 19 central actin filament bundle in the cell process.

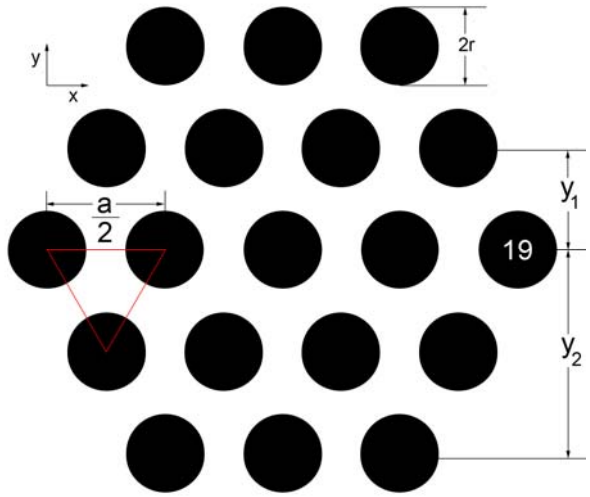

$$I_a = \frac{1}{4}\pi r^4 \quad \text{(D1)}$$

$$I_b = \sum (I_a + A_a \cdot y_1^2) + \sum (I_a + A_a \cdot y_2^2) \quad \text{(D2)}$$

$$I_b = 8 \cdot \left(I_a + \pi r_a^2 \cdot \left(\frac{\sqrt{3}a}{4} \right)^2 \right) + 6 \cdot \left(I_a + \pi r_a^2 \cdot \left(\frac{\sqrt{3}a}{2} \right)^2 \right) \quad \text{(D3)}$$

$$I = I_b \quad \text{(D4)}$$

D.2. Bending analysis of cell process using elastic beam theory

Elastic beam theory may be applied to relate the measured deflection δ_m of the cell process midway between rigid attachment points and force applied to the cell process. The distance L between integrin attachment sites, where there was no observed deflection, was measured from light images of the cell process during SFSP application. The Young's modulus of a single actin filament with bound tropomyosin, E=2612 pN/nm^2, is carefully measured using nanomanipulation (Kojima et al., 1994). The area moment of inertia of the 19 filament central actin bundle is calculated to be I=8.6x10^4 nm^4.

The relationship between the force acting at the midpoint between attachment sites and the local deflection is given by:

$$\delta_{0<x<\frac{L}{2}} = \frac{Fx}{48EI}\left(3L^2 - 4x^2\right). \qquad \text{(D5)}$$

The maximum deflection at x = L/2 is given by:

$$\delta_m = \frac{FL^3}{48EI} \ . \qquad \text{(D6)}$$

δ_m is obtained from the measured maximum displacement of the cell process from its initial position as shown in **Figure S2**, scale bar is 5 μm**.**

Figure S2: Measurement of maximum cell process deflection

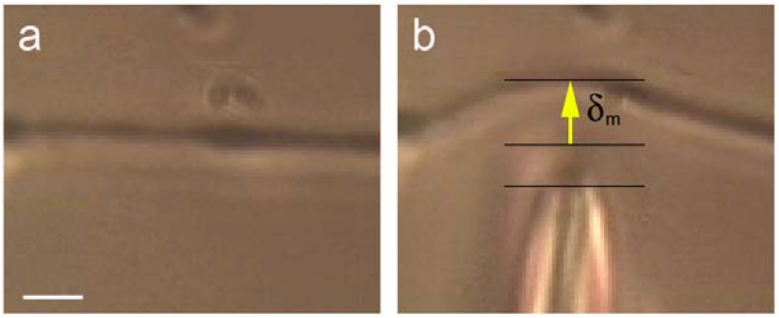

D.3. Force on cell process is treated as a concentrated force

In the above analysis, the force F is treated as a concentrated as opposed to distributed force. A rough approximation to the lateral force distribution can be obtained from the Sampson pressure field given by Equation (C2), at varying distances *z* from the SFSP tip. These lateral profiles are plotted in **Figure S3**, where the radius of the pipette tip *c* is 0.4 μm**.** The force is treated as a concentrated load because of the rapid lateral decay in pressure from the centerline compared to the distance *L* between focal attachment sites, see **Table 2**. The theoretically predicted forces, based on Equation (D6) and their corresponding cell process deflections are shown in **Table 2** in the main manuscript.

Figure S3: Theoretical pressure distributions at varying distances from the pipette tip

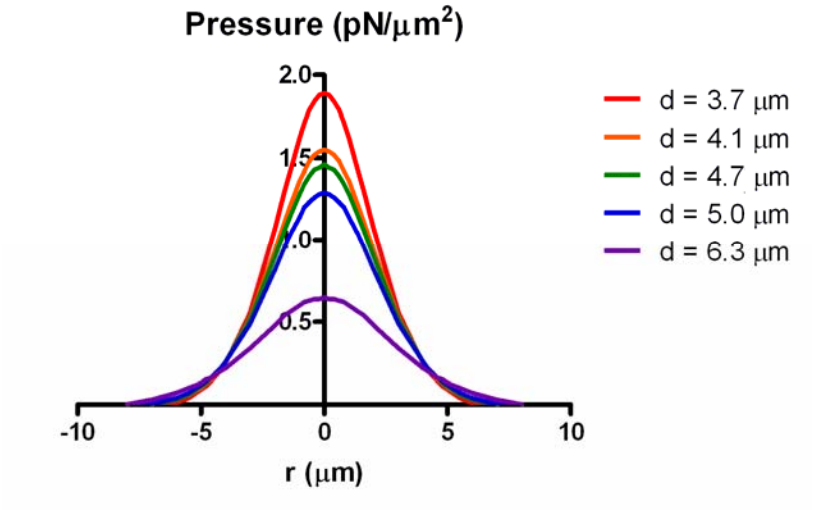

Appendix E

Image series of the expanding bolus when backfilled with high MW dextran conjugated fluorescein (MW 70,000) to mitigate diffusional spreading. Yellow boundary was more clearly defined than with Lucifer yellow dye, but blurring still existed and time intervals were still too long to accurately measure expansion of bolus or clearly define its edge. Back pressure of 20 psi was applied for 100ms. Both greyscale fluorescent and pseudo color images are shown. Scale bar is 50 μm.

Figure S4 – Tracer study using dextran conjugated fluorescein (MW 70,000)

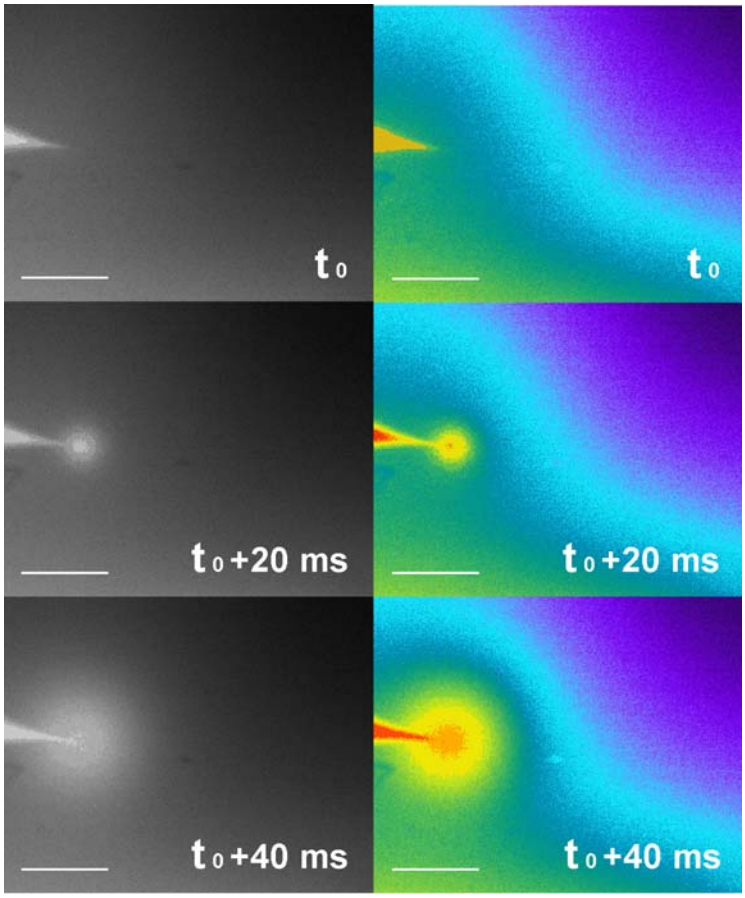

References

Allison, D. P., Hinterdorfer, P., and Han, W., 2002. Biomolecular force measurements and the atomic force microscope. Current Opinion in Biotechnology 13**,** 47-51.

Bausch, A. R., Ziemann, F., Boulbitch, A. A., Jacobson, K., and Sackmann, E., 1998. Local measurements of viscoelastic parameters of adherent cell surfaces by magnetic bead microrheometry. Biophysical Journal 75**,** 2038-2049.

Binnig, G., Quate, C. F., and Gerber, C., 1986. Atomic force microscope. Physical Review Letters 56**,** 930-933.

Bohnet, S., Ananthakrishnan, R., Mogilner, A., Meister, J. J., and Verkhovsky, A. B., 2006. Weak force stalls protrusion at the leading edge of the lamellipodium. Biophysical Journal 90**,** 1810-1820.

Evans, E. and Ritchie, K., 1997. Dynamic strength of molecular adhesion bonds. Biophysical Journal 72**,** 1541-1555.

Evans, E., Heinrich, V., Leung, A., and Kinoshita, K., 2005. Nano- to microscale dynamics of p-selectin detachment from leukocyte interfaces. I. membrane separation from the cytoskeleton. Biophysical Journal 88**,** 2288-2298.

Hu, S., Eberhard, L., Chen, J., Love, J. C., Butler, J. P., Fredberg, J. J., Whitesides, G. M., and Wang, N., 2004. Mechanical anisotropy of adherent cells probed by a three-dimensional magnetic twisting device. AJP - Cell Physiology 287**,** C1184-C1191.

Huang, H., Kamm, R. D., and Lee, R. T., 2004. Cell mechanics and mechanotransduction: pathways, probes, and physiology. AJP - Cell Physiology 287**,** C1-11.

Hughes, S., El Haj, A. J., and Dobson, J., 2005. Magnetic micro- and nanoparticle mediated activation of mechanosensitive ion channels. Medical Engineering & Physics 27**,** 754-762.

Kojima, H., Ishijima, A., and Yanagida, T., 1994. Direct measurement of stiffness of single actin filaments with and without tropomyosin by in vitro nanomanipulation. Proceedings of the National Academy of Sciences of the United States of America 91**,** 12962-12966.

Litvinov, R. I., Vilaire, G., Shuman, H., Bennett, J. S., and Weisel, J. W., 2003. Quantitative analysis of platelet $\alpha_v\beta_3$ binding to osteopontin using laser tweezers. Journal of Biological Chemistry 278**,** 51285-51290.

Ounkomol, C., Xie, H., Dayton, P. A., and Heinrich, V., 2009. Versatile horizontal force probe for mechanical tests on pipette-held cells, particles, and membrane capsules. Biophysical Journal 96**,** 1218-1231.

Simon, A. and Durrieu, M. C., 2006. Strategies and results of atomic force microscopy in the study of cellular adhesion. Micron 37**,** 1-13.